The Potential Impact of Primordial Black Holes on Exoplanet Systems

Garett Brown,[1] Linda He,[2] and James Unwin[3,4,5]

[1] *Department of Physics, University of Toronto, Toronto, Canada.*
[2] *Massachusetts Institute of Technology, MA, USA.*
[3] *Department of Physics, University of Illinois Chicago, Chicago, IL 60607, USA.*
[4] *Rudolf Peierls Centre for Theoretical Physics, University of Oxford, Oxford OX1 3PU, UK.*
[5] *Queen's College, Oxford OX1 4AW, UK.*

ABSTRACT

The orbits of planetary systems can be deformed from their initial configurations due to close encounters with large astrophysical bodies. Candidates for close encounters include astrophysical black holes, brown dwarf stars, rogue planets, as well as hypothetical populations of primordial black holes (PBH) or dark matter microhalos. We show that potentially tens of thousands of exoplanetary systems in the Milky Way may have had close encounters with PBH significant enough to impact their planetary orbits. Furthermore, we propose that precision measurements of exoplanet orbital parameters could be used to infer or constrain the abundances of these astrophysical bodies. Specifically, focusing on PBH we numerically estimate the number of times that such objects pass through the local neighborhood of a given planetary system, and then analyze the statistical impact on the orbital parameters of such systems.

1 INTRODUCTION

Recent technological advancements relating to searches for exoplanets have led to significant developments in our understanding of the composition and formation of planetary systems e.g. (Wright et al. 2011; Thompson et al. 2018). However a number of critical questions remain to be answered, of particular interest is how late time planetary orbits may be shaped due to interactions between planetary systems and transient close encounters with astrophysical bodies which intrude into the radius of influence of the parent star. Such close encounters quite naturally occur with other stars and free floating planets, in this work we extend these considerations to consider more exotic hypothetical astrophysical bodies. One reason that populations of exotic objects are interesting is due to the fact that their typical mass scale, spatial distribution, and velocity dispersions may be very different to conventional objects such as stars and planets. Not only may a population of exotic bodies be able to explain variations in the orbits of exoplanets, but precision studies of exoplanetary orbital parameters can potentially constrain (or favor) the existence of new populations of astrophysical bodies, beyond stars and rogue planets.

The solar system contains many free-floating bodies which can potentially behave intrude on a stellar system, including unbound comets, free floating planets, planetesimals, stars, brown dwarf stars, astrophysical black holes, as well as hypothetical populations of substellar mass primordial black holes or dark matter microhalos. The aim of this work is to examine how the eccentricity and semimajor axis distributions for exoplanetary systems may be impacted by encounters with such astrophysical objects.

Here we take Primordial Black Holes (PBH) as our quintessential example of an exotic astrophysical object. PBH are black holes which form not through stellar collapse, but rather from extreme over-densities in the early universe (Zel'dovich & Novikov 1967; Hawking 1971), as such PBH can potentially have masses well below one Solar Mass $M_\odot$. While we will phrase our study in terms of PBH, our conclusions should be robust for other compact massive objects since the results are entirely set via their gravitational influence. Examples of other comparable hypothetical bodies includes: ultracompact dark matter microhalos, axion minihalos, and dark matter stars (Hogan & Rees 1988; Berezinsky et al. 2013; Freese et al. 2015).

In many cases the interaction of a planet-star system with its environment can be reduced to a gravitational three-body problem. One such situation is when the third body acts as a passing flyby, perturbing the planet-star system. In particular, the passing flyby exchanges energy with the planet-star system, perturbing the orbit of the planet. Other scenarios include collision between the passing flyby with the planet or the dissociation of the planet-star system (Cuello, Ménard, & Price 2022; Moore, Li, & Adams 2020; Hills 1975). The natural starting point is to compare to existing literature on close encounters between stellar systems and intruder stars. In particular, Adams & Li (Li & Adams 2015) have investigated changes in planet eccentricities due to close encounters with binary stars, and Heggie & Spurzem (Spurzem et al. 2009) have studied the analytical estimates of the changes in planet orbital eccentricity and semimajor axis due to stellar adiabatic and impulsive encounters. In this paper, we extend the study of stellar encounters to passing flybys of different initial parameters than that of

stars. In the case of PBHs, because these objects form prior to galaxy formation, it is a reasonable expectation that the PBHs to have the same velocity dispersion as dark matter. Since the mean of the dark matter velocity dispersion is 220 km/s (Navarro et al. 1996), the case of PBH can be highly distinct to the stellar case (with mean of ~ 40 km/s). Accordingly, high velocity flybys with PBHs are categorized as 'impulsive encounters' Spurzem et al. (2009).

Though the first exoplanet around a main sequence star was discovered in 1995 (Mayor & Queloz 1995), there are now well over 5000 confirmed exoplanets in thousands of systems (exoplanet.eu). These planets span a wide range of (dynamical) masses, semimajor axes, eccentricities, and other orbital elements. However, due to observational bias, there is not a complete picture on the distributions of the orbital elements of exoplanets (Burke et al. 2015; Christiansen et al. 2016). With these biases, in the current population of known exoplanets Jupiter-like planets are the most common, in part because they are the easiest to detect. Furthermore, the most successful detection method, the transit method, is heavily biased towards short period planets. As such, the most common semimajor axes of known exoplanets are within 1 AU. Additionally, there is still much to understand regarding the connections between proto-planetary disks and the features of known exoplanet systems (Mulders et al. 2020; Emsenhuber et al. 2021).

The rich and complex possible histories of dynamical evolution complicate matching disk simulations to the population of established planetary systems. The commonly observed (mostly) circular orbits are likely the result of the dynamics involved in formation including dynamical friction (Chandrasekhar 1943), migration, and tides. Also, the connection between stellar mass and common formation location (semimajor axis) of planets is not fully understood. Therefore, since neither observations nor simulations currently give complete or accurate predictions for initial values, we will estimate the eccentricity and semimajor axis distributions for exoplanetary systems, with the assumption that the initial eccentricity and semimajor axis of all the planets are Jupiter-like with $(e_0, a_0) \sim (0, 10 \text{ AU})$. Thus, our aim is to identify the late time values of $e_\infty = e_0 + \Delta e$ and $a_\infty = a_0 + \Delta a$ acknowledging that these perturbations Δa and Δe receive a contribution from standard astrophysical sources, such as close encounters with stars, as well as potentially from encounters with hypothetical bodies such as primordial black holes. Moreover, one expects that Δa and Δe will depend on the radial distance from the Galactic Centre, since the densities and velocities of stars and PBH will change depending on their position in the galaxy.

This paper is organized as follows: In Section 2, we discuss the role of numerical simulations for studying close encounters with particular reference to PBH. Section 3 describes the approach we employ to estimate the orbital distributions of all exoplanets. We then track the frequency and probability of PBHs entering an appropriate region of the star that could lead to non-negligible orbital changes in Section 4. In Section 5, we present the expected number of exoplanets over the entire galaxy that could experience a significant close encounter with a PBH and the distribution of the eccentricities of such exoplanets. We present our concluding remarks in Section 6.

2 SIMULATING CLOSE ENCOUNTERS

In this first section we first discuss how one can model stellar system flybys, leading to some statistical studies which relate the statistical impact to the planetary orbits for different assumptions regarding the relative mass and velocity of the flyby object, the closest approach of the flyby. Specifically, we shall study the statistics of encounters between a flyby object and a simple planet-star system consisting of a single planet and parent star. The planet-star system consists of a central star with mass M_c and one planet with mass M_1, semimajor axis a, and eccentricity e. We focus on the changes to the eccentricity δe or semimajor axis δa, these can be related to the relative change in binding energy and the angular momentum per unit mass (respectively $\delta E/E$ and $\delta J/J$) as follows (see e.g. (Li & Adams 2015)):

$$\frac{\delta E}{E} = -\frac{\delta a}{a} \,,$$
$$\frac{\delta J}{J} = -\frac{1}{2}\frac{\delta a}{a} - \frac{e \delta e}{1 - e^2} \,. \tag{1}$$

Notably, one parameter that strongly influence the perturbation strength of encounters is the distance of the closest approach, initial speed of the third body relative to the planet-star system, v_∞. If v_∞ is much larger than the orbital speed of the planet, then the encounter is said to be *impulsive*, otherwise, the encounter is called *adiabatic* (Spurzem et al. 2009). In this paper, we put particular attention to the case of impulsive encounters since the velocity of PBHs is expected to be significantly larger than that of the planet.

To carry out simulations of close encounters between passing flybys with planet-star systems, we use the REBOUND (Rein & Liu 2012) software package, an N-body integrator that integrates the motion of particles under the influence of gravity.[1] Specifically, we adapt the package REBOUND to simulate impulsive close encounters. To our knowledge this is the first such numerical study of impulsive close encounters describing PBH flybys.

The set of parameters is the flyby's mass M_*, velocity at infinity relative to the planet-star system v_∞, and impact parameter b_*, along with the initial parameters of the planet-star system, in particular the parent star's mass M_c, and the planet's mass M_1, semimajor axis a, and eccentricity e. We introduce the passing flyby on a hyperbolic trajectory, with mass M_*, eccentricity e_*, impact parameter b_*, and relative velocity v_∞, its closest approach r_p is given by

$$r_p = b_* \sqrt{\frac{e_* - 1}{e_* + 1}} \approx b_* \,. \tag{2}$$

We implement REBOUND using a hybrid integration scheme[2] for switching from WHFast (Rein & Tamayo 2015) to IAS15 (Rein & Spiegel 2015) and back to WHFast if the flyby object passes within 30 AU. If $r_p > 30a$ then REBOUND simply uses WHFast for the entire integration. This hybrid scheme allows for fast integrations and high resolution 3-body interactions because it takes advantage of the predominantly Keplerian motion when the bodies are weakly interacting.

---

[1] Analytical estimates of the eccentricity change and effective cross-sections in terms of the initial parameters of the encounter can potentially be derived, see e.g. (Spurzem et al. 2009).
[2] The code, titled "airball", is available at (Brown 2022).
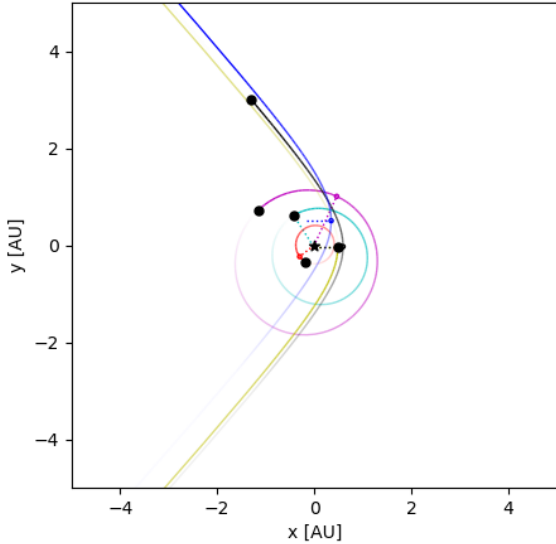
Figure 1. For illustrative purposes only we show here the case of 4 planets on circular orbits around a central star ($\star$), whereas in our main simulations we only consider single planets orbiting stars. The flyby of the intruding body are on hyperbolic trajectories and shown as brown, black and yellow curves.

Our code uses a sufficiently small fixed timestep, between 1 and 5 per cent of the innermost orbital period when integrating with `WHFast`, so that when switching to `IAS15` the change in energy to the system incurred by switching integrators is negligible compared the change in energy of the system due to a flyby. Switching back from `IAS15` to `WHFast` is also done at the same distance away from the planet-star system. The advantage of switching is being able to use the adaptive timestepping of `IAS15` to untangle the close encounters and strong interactions that break the assumptions of the `WHFast` integrator. We initialize `REBOUND` for a flyby object on a hyperbolic trajectory given the flyby's mass, velocity at infinity, and impact parameter. Adding an object to a `REBOUND` simulation with a fully determined initial orbit requires the object's semimajor axis, eccentricity, inclination i, longitude of the ascending node Ω, longitude of perihelion ϖ. Figure 1 graphically illustrates the trajectories traced out under our simulation scheme for a single example run.

For all simulations presented in this paper, unless otherwise specifically stated, the mass of the star in the planet-star system equals $M_c = 1 M_\odot$, and the mass of the planet equals $M_1 = 10^{-3} M_\odot$, with semimajor axis $a = 5$ AU or 10 AU and eccentricity $e = 0$, comparable to that of the Sun-Jupiter/Neptune-like systems. For each set of initial parameters, we implement the Monte Carlo sampling technique to randomly choose the angle orbital parameters of the flyby. In particular, the angular orbital parameters Ω, ϖ, and inclination i of the flyby are all uniformly drawn from a distribution of $[-\pi, \pi]$. Moreover, each initial setup is ran for $N = 10$ samples, with each sample having independently sampled angle orbital parameters. We then perform several large ensembles of numerical scattering simulations to examine the effect of different parameters of the passing flyby on the perturbation strength of the encounter.

In the first set of simulations, we consider the effect of the passing flyby's velocity on the perturbation strength of the close encounter. Accordingly, Figure 2 shows the relative change in energy and change in eccentricity of the planet for surviving planet-star systems due to encounters with passing flybys at approximately zero impact parameter $b_* \approx 0$. The ratio of the flyby's mass to the planet's mass is taken to be

$$R_M \equiv M_*/M_p = 10^{-3}, \ 10^{-1}, \ 10. \qquad (3)$$

The x-axis of Figure 2 shows increasing velocity, in terms of R_v the ratio of the flyby star velocity relative to the orbital velocity of the planet. Each point in Figure 2 corresponds to the average value of 10 simulations. Note that for different values of R_M, the general shape of the curve is highly analogous. Moreover, the values for Δe and $|\Delta E/E|$ are similar. The line of best fit is of the form

$$\alpha_1 \cdot \exp\left(-\gamma_1 \cdot R_v\right) + \beta_1, \qquad (4)$$

we find $\gamma_1 \approx 0.9$ to be a good fit and the values of α_1 and β_1 are highly dependent on the ratio of the flyby mass to the planet mass. Observe that the perturbation strength decreases exponentially with respect to increases in the flyby velocity until the threshold value $R_v \approx 10$, where after the perturbation strength is insensitive to further increases in the flyby velocity. For a Sun-Jupiter system, a flyby of mass $M_* = 10^{-2} M_\odot$ and velocity $v_\infty \approx 130$ km/s can lead to percent level changes in planetary eccentricities ($\Delta e \sim 0.01$).

Figure 3 provides a complementary presentation of the information in Figure 2, in this case we take fixed values of the ratio of velocities R_v and vary the ratio of flyby mass to planet mass along the x-axis. Similarly, each point is the average value of 10 simulations. Note that the data points of all three different flyby velocities lie roughly along the same curve, and the values for Δe and $|\Delta E/E|$ are similar. Due to the stochastic nature of the resulting data points, we present one fitted line for all three flyby velocities. In particular, we found the line of best fit to be of the form $\gamma_2 \cdot R_{M_*}$, with $\gamma_2 \approx 0.001$ being a good fit. We highlight in particular that, the perturbation strength increases linearly with respect to increase in the mass of the flyby. For a Sun-Jupiter system, a flyby of mass $M_* \approx 10^{-1}$ can lead to a $\Delta e \approx 0.1$ increase in the planet's orbital eccentricity.

Figure 4 shows the effect of varying the impact parameter of the flyby. Specifically, we show the relative changes in energy and eccentricity of the planetary orbit for surviving planet-star systems following a a flybys with velocity $v_\infty \approx 200$ km/s. The flyby's mass is taken such that $R_M = 10^{-3}, \ 10^{-1}$, and 10^1. The x-axis shows increasing impact parameter of the flyby in terms of the scaled quantity $R_b \equiv b_*/a$, where a is the initial semimajor axis of the planet. Again, each point is the average value of 10 simulations. We found the line of best fit of the form

$$\alpha_3 \cdot \exp(-\gamma_3 \cdot R_b) + \beta_3, \qquad (5)$$

with $\gamma_3 \approx 0.33$ and the values of α_3 and β_3 are sensitive to R_M. The impact parameter b_* governs the closest approach between the flyby and the parent star, cf. eq. (2). Therefore, the perturbation strength decreases exponentially with respect to increases in the flyby impact parameter. For a Sun-Jupiter system, a flyby with closest approach $b_* \approx 4$ AU and mass $10^{-2} M_\odot$ can lead to $\Delta e \approx 0.01$.
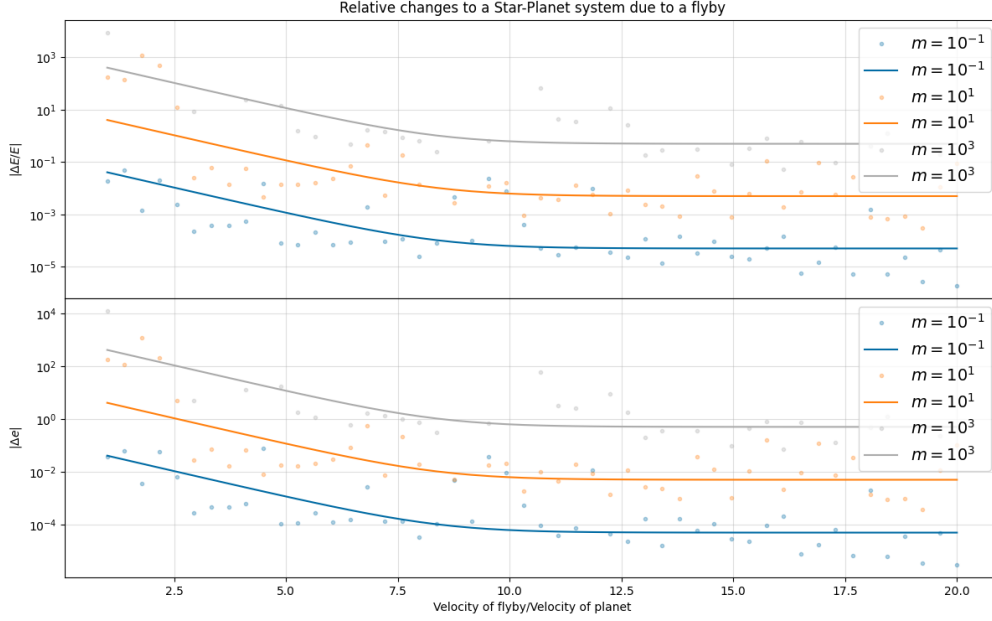
Figure 2. Changes in the relative energy and eccentricity of the planet due to encounters with passing flybys at ≈ 0 impact parameter with the ratio of the flyby's mass to the planet's mass being $R_M = 10^{-3}$, 10^{-1}, and 10^1 respectively. The x-axis shows increasing velocity R_v of the flyby star as a dimensionless value in terms of the orbital velocity of the planet. Each point is the average value of 10 simulations.
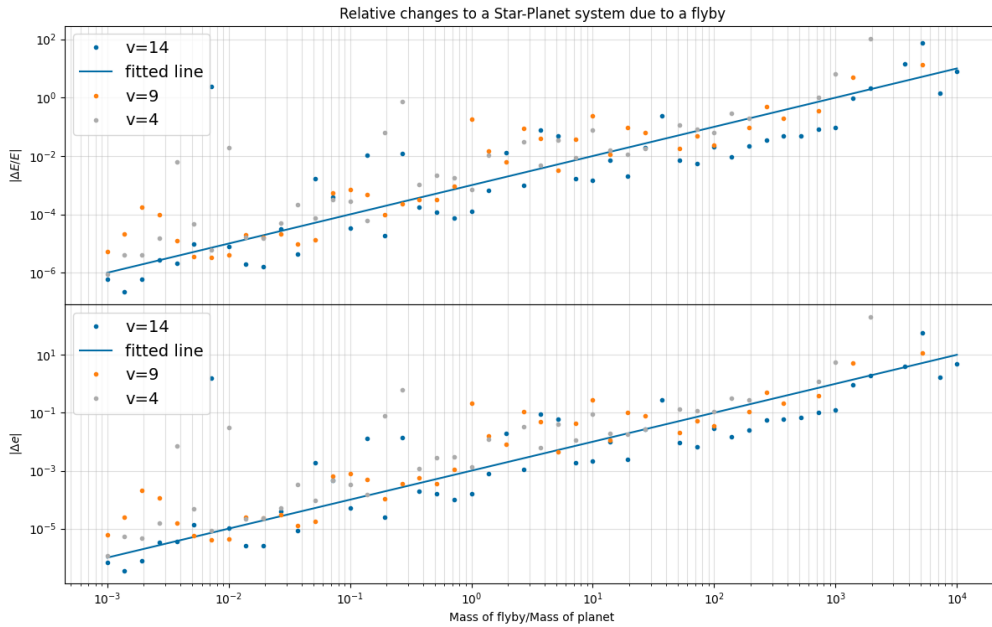
Figure 3. Changes in the relative energy and eccentricity of the planet due to encounters with passing flybys at ≈ 0 impact parameter with the ratio of the flyby's velocity to the planet's mass being $R_v = 14$, 9, and 4 respectively. The x-axis shows increasing mass R_{M_*} of the flyby star as a dimensionless value in terms of the mass of the planet. Each point is the average value of 10 simulations.
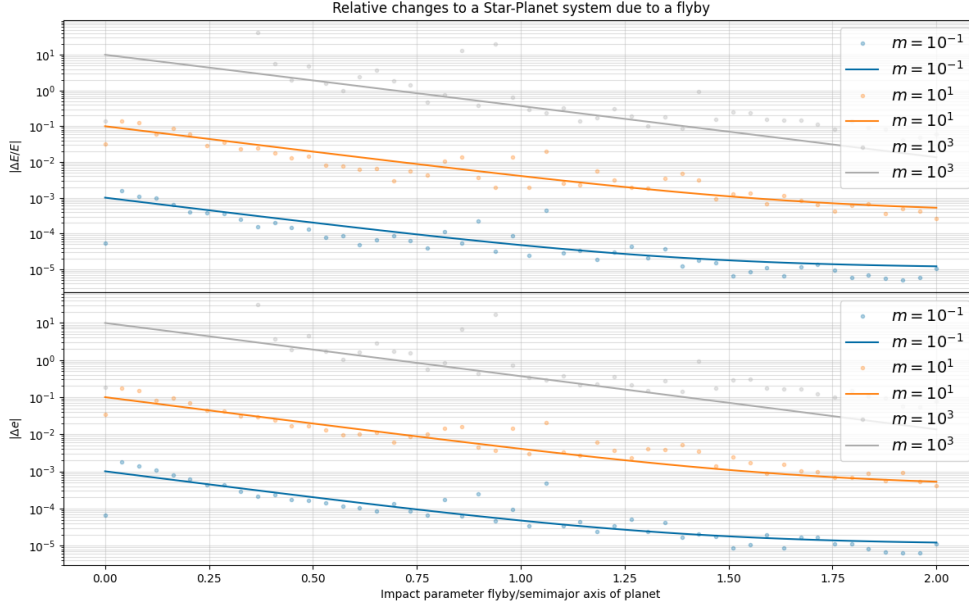
Figure 4. Changes in the relative energy and eccentricity of the planet due to encounters with passing flybys of velocity $v_\infty \approx 200$ km/s, with the flyby mass to the planet mass ratio being $R_M = 10^{-3}$, 10^{-1}, or 10^1. The x-axis shows increasing impact parameter R_b of the flyby star as a dimensionless value in terms of the semimajor axis of the planet. Each point is the average value of 10 simulations.

## 3 TRACKING DYNAMICS ACROSS 10 ORDERS OF MAGNITUDE

The previous section generalizes the statistics of the changes in the semimajor axis and eccentricity of the planet given a close encounter. In principle, if one can estimate the number of close encounters throughout the galaxy, then this would lead to predictions of the distributions of eccentricities and semimajor axes of exoplanets. As a first step towards this, this work aims to understand the expected distribution of exoplanet orbital parameters under a number of simplifying assumptions. Our first assumption is that all exoplanets are simple star-planet systems with mass $10^{-3}M_\odot$ and initial orbital parameters $(e_0, a_0) \sim (0, 10\text{ AU})$. Our analyses are likely reasonable for modeling impact on systems with a single large planet, if such systems also have small bodies they are unlikely to significantly perturb the analysis. The starting configuration $(e_0, a_0) \sim (0, 10\text{ AU})$ is likely an oversimplification since we expect formation histories may impact a_0 and stellar encounters likely smear this distribution.

There are essentially two ways in which planetary orbital parameters could be perturbed by intruding objects to a stellar system:

1. Intruder passes through the system without being captured, i.e. a one time event, referred to as a 'flyby'.

2. Intruder is captured by the system, potentially leading to multiple interactions between planets and the intruder.

In this work we focus on scenario 1, noting that while capture may be more impactful since it necessarily involved energy dissipation via a three-body interaction it is statistically extremely unlikely to occur compared to flyby events.
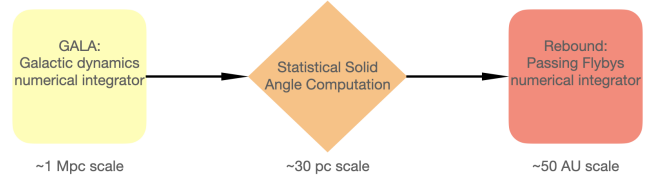
Figure 5. Flow diagram showing the chain of dedicated code applied in order to study how primordial black holes (PBHs) influence the orbits of exoplanets. We also indicate the typical length scale at which the simulation is targeted.

Taking scenario 1, a quantitative assessment can essentially be broken into three sub-questions:

A. Given a star in a circular orbit around the Galactic Center, what is the frequency to which some PBH in the galaxy enters the neighborhood of the given star?

B. Given a PBH enters the neighborhood of a star, what is the probability that this PBH enters a region in which it can significantly perturb the orbits of the star's planet(s)?

C. Given a PBH that enters the planet perturbing region, statistically what are the effects on the orbital parameters?

In this manner we will ascertain whether PBH (or similar objects) can significantly impact the orbits of exoplanets across the Milky Way. Note that Section 2 gives the statistical results on the changes in the orbital parameters (eccentricity and semimajor axis) of the planet in terms of three parameters of the flyby PBH, so it remains to answer questions **A** and **B**, and then to look at the statistical distributions of exoplanet orbits, as we do over the remainder of this paper.
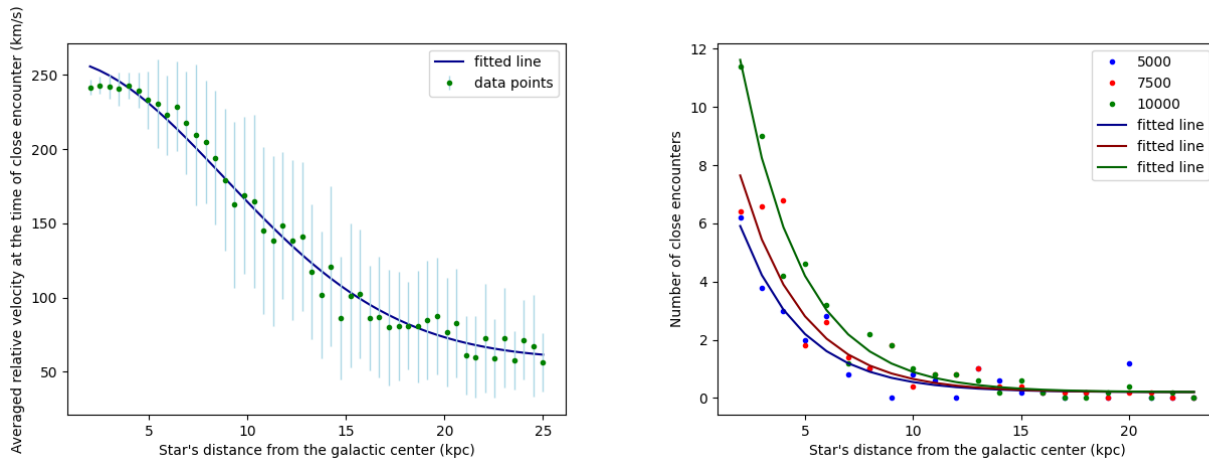
Figure 6. GALA outputs. Left. Averaged relative velocity (km/s) between the PBH and the star at the time of close encounter. Each point is the average of 240 simulations. Right. Number of close encounters as a function of the star's distance r from the Galactic Center within the region of longitude between $(-\theta(r), 2\theta(r))$ and latitude $(-2l(r), 2l(r))$ plotted for different assumptions on the galactic population of PBHs (5000, 7500, or 10,000).

To accomplish this study, we break the analyses into three stages (corresponding to **A**, **B** and **C**). For part **A**, to estimate the number of PBH which enter the neighborhood of a given star—which we take to be a sphere of radius $r_n = 30$ pc—we implement numerical galactic dynamics simulations using the public GALA code (Price-Whelan 2017). GALA models the PBHs and the given star as test particles and traces out the trajectories of the test particles based on a given mass model potential.

We then compute the probability that a PBH in the neighborhood of a star has the appropriate trajectory such that its perturbation of planetary orbits is non-negligible, typically coming within 15 AU (for Jupiter-like planets) and 90 AU (for Neptune-like planets) of the star, thus addressing **B**. When computing the probability that the PBH enters the solid angle in question **B**, the PBH's initial distance from the star at a distance $d < r_n = 30$ pc (introduced in our GALA analysis) with the exact value d drawn from a distribution of distances at the time of close encounter from the galactic simulations. We defined the solid angle sphere of region to be the sphere with radius $r_c = 200$ AU around the star. These computations are detailed in Section 4.

For question **C**, to build on the results obtained in Section 2, the REBOUND simulations use the results of the solid angle code to sample how the close encounters play out, specifically we consider the impact parameters of the PBH to be $b_* < r_c$ and examine the flyby's effect on the planet's orbital parameters. Section 5 describes this process in detail.

This three-step numerical study is important to be able to make the problem computationally tractable. Note that the scale of the galaxy is ~ 1 Mpc, while stellar systems are of order 10^{-4} parsec (this is the Neptune-Sun distance), thus the problem spans 10 orders of magnitude in distances. Compartmentalizing the problem into three units essentially tracks the relevant dynamics first at the Galactic scale using GALA, then at the parsec scale via our custom solid angle simulator, then finally at the interplanetary scale $\lesssim 50$ AU using REBOUND. Figure 5 shows the flow diagram of the above-mentioned approach. To our knowledge 'daisy-chaining' of these codes in this fashion has not been previously explored.

4   SIMULATING GALACTIC DYNAMICS

Numerically, to determine the frequency of PBHs and other classes of astrophysical objects entering the neighborhood of a given star, we implement galactic simulations using the public code GALA. This Astropy-affiliated Python package numerically integrates the trajectories of stars and other astrophysical objects based on a given mass model. In particular, we use the MilkyWay Potential model, consisting of a spherical nucleus and bulge, a Miyamoto-Nagai disk, and a spherical NFW dark matter halo.

A test particle, representing the given star, is placed at a distance between 2 kpc and 25 kpc from the Galactic Center, with initial circular velocity orbiting around the Galactic Center at 100 km/s. For a given star r kpc away from the Galactic Center, we specify a region of interest, i.e. a solid angle, of the entire sphere by computing the maximal latitudinal and longitudinal angles this star with 100 km/s can travel in 1 Myr. Then 10^4 test particles, representing the primordial black holes, are randomly placed across the galaxy with longitudes spanning from $(-\theta(r), 2\theta(r))$ and latitudes spanning from $(-2l(r), 2l(r))$, where $\theta(r)$ is the angle this star can traverse in 1 Myr and $l(r)$ is the maximum latitude this star can traverse in 1Myr. We assume the PBH follow the density profile of dark matter, and so the distribution of the 10^4 test particles (spanning from 1 to 30 kpc from the Galactic Center) are based on the NFW (Navarro-Frenk-White) density profile (Navarro et al. 1996). Moreover, each PBH is assigned a starting speed of 220 km/s and a randomized direction. We calculate the average number of close encounters within the specified region as a function of the star's distance r from the Galactic Center and then rescale this to account for the entire galaxy.

We implement the integration using the Leapfrogintegrator, a symplectic integrator that computes the position coordinates and velocity vectors of particles with specified timesteps. For each time step, we evaluate the pairwise distances between the given star and each of the PBH, and evaluate the relative velocity
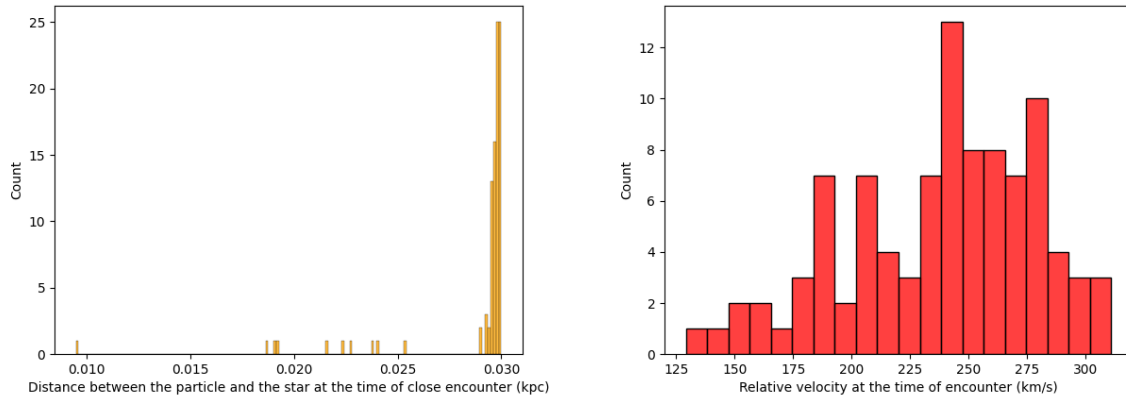
Figure 7. GALA outputs. Left. Histogram of the distances between the PBH and the star at the timestep when the PBH is within distance r_n of the star. The result is taken from a total of 12 simulations, 3 of each star's initial distance from the Galactic Center being $2, 3, 4, 5$ kpc. Right. Histogram of the relative velocities between the PBH and the star at the timestep when the PBH is within distance r_n of the star. The result is taken from a total of 12 runs, 3 for each star's initial distance from the Galactic Center being $2, 3, 4, 5$ kpc.

between the two objects if the primordial black hole is within distance r_n of the star. We take $r_n = 30$ pc.

Figure 6 shows the result of the averaged relative velocity (km/s) between the PBH and the star at the time of close encounter. The curve follows the gaussian distribution, and a gaussian fitting gives the line of best fit to be $\alpha \cdot \exp(-\beta \cdot (r^2)) + \gamma$, with $\alpha \approx 203$, $\beta \approx 0.0065$, and $\gamma \approx 57.8$ being a good fit. Notably is the smaller values of the velocity at large values of r. Since the perturbation strength decreases exponentially with respect to increase in flyby velocity (Section 2), smaller velocity means that each close encounter would lead to a larger perturbation strength.

Figure 7 shows the distributions of distances between the PBH and the star at the timestep when the PBH is within distance r_n of the star (left) and the relative velocities between the PBH and the star at the time of the close encounter (right). This is calculated from a total of 12 simulations, 3 of each star's initial distance from the Galactic Center being $2, 3, 4, 5$ kpc. The distribution of such distances paves the ground for the solid angle probability calculation, where we randomly sample the starting distances between the PBH and the star from this distribution.

The above analysis with GALA gives the frequency of PBHs coming within distance $d < r_n = 30$ pc of the star and the distribution of the exact distances at the time of close encounter. We next statistically compute the probability that a PBH in the neighborhood of a star ($d < r_n = 30$ pc) has the appropriate solid angle region such that its perturbation of planetary orbits is non-negligible, typically coming within 15 AU (for Jupiter-like planets) and 90 AU (for Neptune-like planets) of the star. This distance is different for Jupiter and Neptune because of their different semimajor axes.

Figure 8 (left) provides a graphical representation of the scenario. For each simulation, the PBH's initial distance from the star, $d < r_n = 30$ pc, (introduced in our GALA analysis), is randomly drawn from a distribution of distances at the time of close encounter from the galactic simulations (cf. Figure 7). Since we are interested in cases where the PBH in the neighborhood of a star has the appropriate solid angle region within a sphere with radius $r_f \ll 200$ AU, we re-

strict the PBH's velocity vector v to be aiming at a specified region of the sphere with solid angle $\approx 2.5 \cdot 10^{-8}$ steradians (to simplify our calculations). We later rescale to obtain the full probability for randomly distributed components. Given the afore-mentioned sampling scheme, we then compute the closest distance between the PBH and the star along the trajectory of the PBH.

Figure 8 (right) demonstrates the probability that a PBH in the neighborhood of the star enters a sphere of radius r of the star. The x-axis is such sphere's radius r, and the y-axis is this probability. However, since we constrained the magnitude of PBH's velocity vector pointing directly to the origin, we must multiply the resulting probability by $4 \cdot 10^{-10}$. For Jupiter-like planets, we found the PBH having a $\approx 5.85 \cdot 10^{-13}$ probability entering a sphere of radius 15 AU around the planet, and for Neptune-like planets, we found a PBH have a $\approx 1.7 \cdot 10^{-11}$ probability entering a sphere of radius 90 AU around the planet.

5 DISTRIBUTIONS OF EXOPLANET ORBITS AFTER A SINGLE PBH ENCOUNTER

The previous two sections give the result of the frequency of close encounters and the probability that such encounters lead to the PBH entering the appropriate solid angle region such that its perturbation of planetary orbits is non-negligible. It remains to compute the changes to the eccentricity and semimajor axes of planets after the PBH enters the appropriate solid angle region.

For Sun-Jupiter systems, the impact parameter (b_*) of the flyby dictates the distance of closest approach and is drawn from a distribution of $15\sqrt{R[0,1]}$AU, such that the sampling is uniform for the cross-sectional area. For Sun-Neptune systems, the impact parameter (b_*) is drawn from a distribution of $90\sqrt{R[0,1]}$AU. We simulate the flybys analogously to the process explained in Section 2 using REBOUND. A detailed analysis could take into account the relative velocities. However, since the bulk of the galaxy (0-20 kpc) has relative velocities between the PBH and the star be-
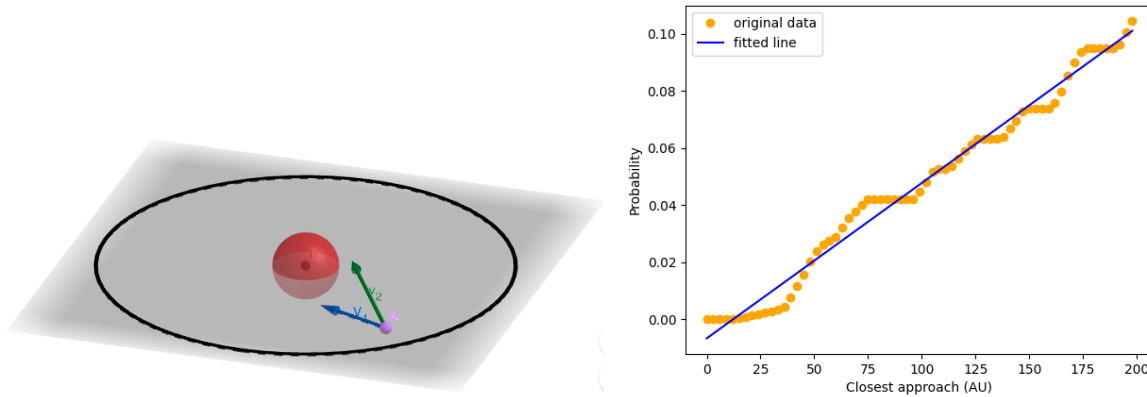
Figure 8. Left. Graphical representation of the solid angle computation scenario. Object A represents the PBH, and we randomly select the velocity vector v of the PBH and its initial distance from the distance distributions extracted from the GALA galactic simulations. We then evaluate the probability that a large sampling of such objects can enter a smaller sphere of region around the star. Right. The probability that a PBH with initial velocity vectors and initial distance from the star randomly sampled enters a sphere with a radius r less than 200 AU around the star as a function of the radius r of the sphere. The result is taken over a total of 10^5 simulations.

tween $60 - 250$ km/s, corresponding to the flat region in Figure 2, the relative changes in energy are insensitive to changes in the relative velocity for most parts of the galaxy. As an initial study, we will take the velocity of the flyby to be 100 or 200 km/s going forward to make the analysis more tractable.

Since there are $\sim 10^{11}$ stars in the Milky Way, and it is expected that almost of these may have exoplanets, then assuming that the stars are uniformly distributed, we may calculate the expected number of exoplanets that experience a significant close encounter with a PBH that non-negligibly alters its orbital parameters. Figure 9 shows the expected cumulated number of exoplanets that experience such an encounter as a function of the distance from the Galactic Center.

To determine the distribution of the eccentricity and semimajor axis of all exoplanets, it remains to determine the probability $p(r)$ of exoplanets of distance r from the center of the galaxy encountering a PBH entering the appropriate solid angle region such that its perturbation of planetary orbits is non-negligible. Then a fraction $(1 - p(r))$ of the exoplanets at distance r from the Galactic Centre have eccentricity e_0, while the remaining $p(r)$ of the exoplanets will have $e \neq e_0$ distributed according to the histogram of eccentricities given in Figure 10 (assuming $e_0 = 0$).

6   CONCLUSION

In this paper, we studied the statistics of the eccentricity and semimajor axis distributions of exoplanets throughout the galaxy looking through the lens of exoplanet's close encounters with surrounding astrophysical objects. In particular, we used the primordial black holes as the example astrophysical object. We estimated the number of Neptune-like and Jupiter-like exoplanets in the galaxy that has encountered a primordial black hole that non-negligibly affected its orbital parameters over the lifetime of the galaxy and the distributions of the resulting orbital parameters. To ob-

tain the values and distributions, we employed three classes of numerical simulations and semi-analytical estimates. We also extended previous analytical and numerical results on the perturbation strengths due to stellar encounters to a wider range of parameters of the flyby. In the appendix, we also include our numerical results extending the parameter space to the parameters of the planet to account for more variability of the mass, eccentricity, and semimajor axis of all exoplanets.

The benefit of the project is two-fold. Firstly, by providing the predicted orbital distributions of all exoplanets, this project can potentially help the Kepler mission in searching for earth-like exoplanets across the Milky Way. Secondly, with the recent deployment of the revolutionary James Webb Space Telescope, astronomers project that a plentitude of new exoplanets will be discovered in the coming decade. Once a comprehensive catalogue of exoplanets and their orbital parameters has been collated, the methodology developed here might be applied to this large dataset as a means to test for the existence of populations of primordial black holes and other astrophysical objects.

Acknowledgements

APPENDIX A: APPENDIX

Figure A1 (left) shows the changes in the relative energy and eccentricity of the Sun-Jupiter system due to encounters with passing flybys of velocity ≈ 200 km/s with impact parameter drawn from a distribution of $15\sqrt{R[0,1]}$AU. The x-axis shows increasing mass M_* of the flyby PBH. Figure A1 (right) presents analogous results for Sun-Neptune systems, such that the impact parameter is drawn from
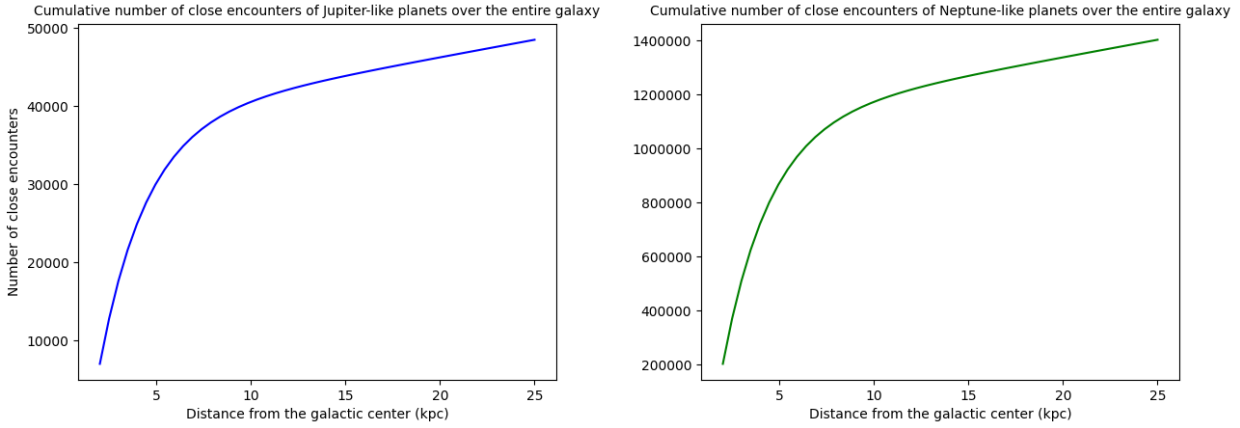
Figure 9. Left. Given 10^9 initial PBHs over the entire galaxy, the expected cumulative number of Jupiter-like planets within distance r from the center of the galaxy that encounters a PBH within 15AU over the age of the galaxy (≈ 10 billion years). Right. Given 10^9 initial PBHs over the entire galaxy, the expected cumulative number of Neptune-like planets within distance r from the center of the galaxy that encounters a PBH within 15AU over the age of the galaxy (≈ 10 billion years).
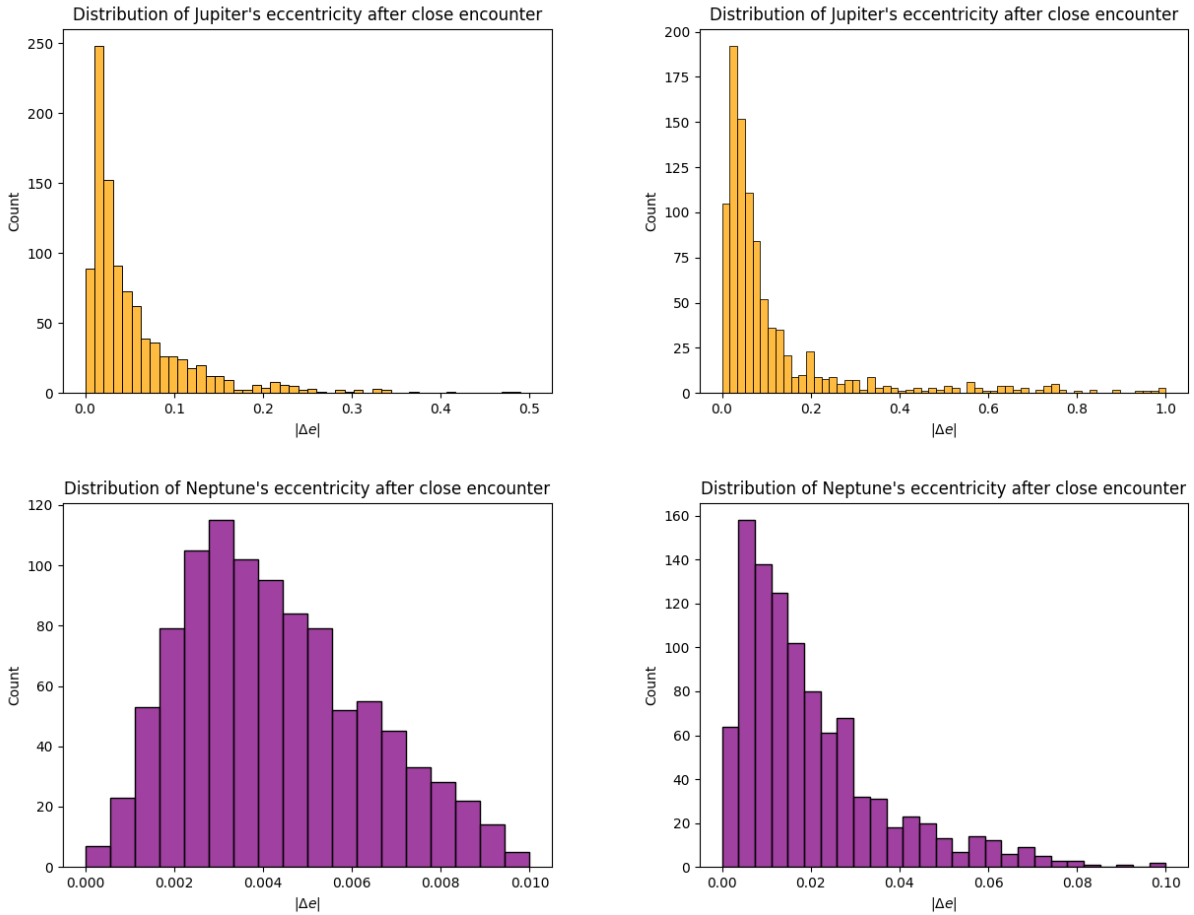

Figure 10. Top left. Distribution of the resulting eccentricities of Jupiter after close encounter with a flyby PBH of mass $10^{-1} M_\odot$ and velocity 200 km/s, with impact parameter drawn from a distribution of $15\sqrt{R[0,1]}$AU. Top right. Distribution of the resulting eccentricities of Jupiter after close encounter with a flyby PBH of mass $10^{-1} M_\odot$ and velocity 100 km/s, with impact parameter drawn from a distribution of $15\sqrt{R[0,1]}$AU. Bottom left. Distribution of the resulting eccentricities of Neptune after close encounter with a flyby PBH of mass $10^{-1} M_\odot$ and velocity 200 km/s, with impact parameter drawn from a distribution of $90\sqrt{R[0,1]}$AU. Bottom right. Distribution of the resulting eccentricities of Neptune after close encounter with a flyby PBH of mass $10^{-1} M_\odot$ and velocity 100 km/s, with impact parameter drawn from a distribution of $90\sqrt{R[0,1]}$AU.

$90\sqrt{R[0,1]}$AU. In both cases each point is the average value of 1000 simulations. Furthermore, Figure 10 gives the distribution of the changes in Jupiter's and Neptune's eccentricities for 1000 close encounters with PBH of mass $10^{-1}M_{\odot}$ and velocities of 100 or 200 km/s, Appendix A.1 indicates how varying the planet's mass, initial eccentricity or semimajor changes these results.

Furthermore, Figure A2 shows the perturbation strength of the close encounter as a function of the initial eccentricity, and semimajor axis.
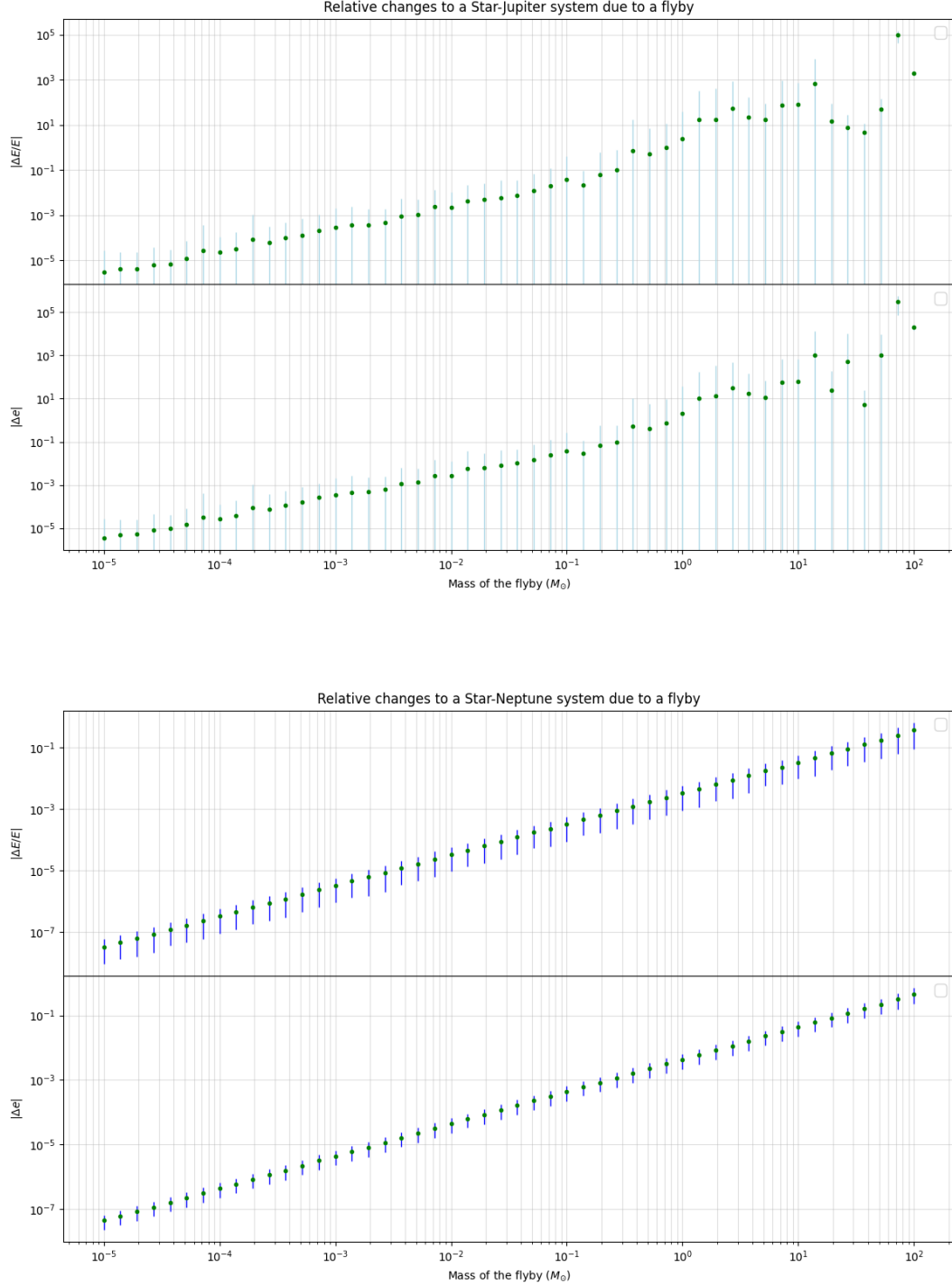
Figure A1. Left. Changes in the relative energy and eccentricity of the Sun-Jupiter system due to encounters with passing flybys of velocity ≈ 200 km/s with impact parameter drawn from a distribution of $15\sqrt{R[0,1]}$AU. The x-axis shows increasing mass M_* of the flyby PBH. Each point is the average value of 1000 simulations. Right. Changes in the relative energy and eccentricity of the Sun-Neptune system due to encounters with passing flybys of velocity ≈ 200 km/s with impact parameter drawn from a distribution of $90\sqrt{R[0,1]}$AU. The x-axis shows increasing mass M_* of the flyby PBH. Each point is the average value of 1000 simulations.
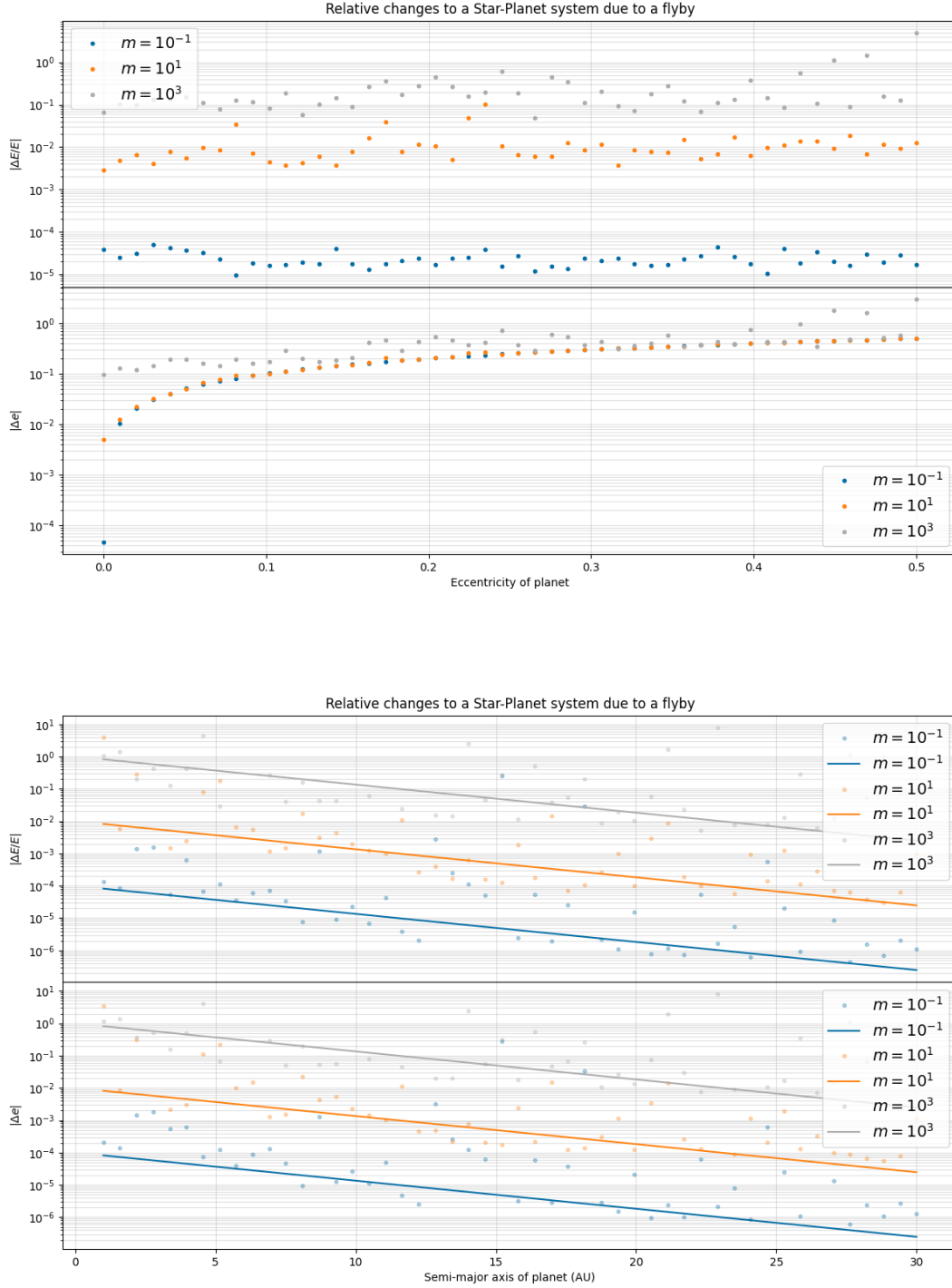
Figure A2. Changes in the relative energy and eccentricity of the planet due to encounters with passing flybys of velocity $v_\infty \approx 200$ km/s with the ratio of flyby's mass to the planet mass being $R_M = 10^{-3}$, 10^{-1}, and 10^1. Each point is the average of 10 simulations. Top. The x-axis shows increasing eccentricity of the planet. Bottom. The x-axis shows increasing semi-major axis of the planet.

REFERENCES

Thompson S. E., *et al.* "Planetary Candidates Observed by Kepler. VIII. A Fully Automated Catalog With Measured Completeness and Reliability Based on Data Release 25" 2018, ApJS, 235, 38.

Wright J. T., *et al.* "The Exoplanet Orbit Database". 2011, PASP, 123, 412.

Hawking S., "Gravitationally collapsed objects of very low mass," Mon. Not. Roy. Astron. Soc. **152** (1971), 75

Y. B. Zel'dovich and I. D., Novikov "The Hypothesis of Cores Retarded during Expansion and the Hot Cosmological Model," Soviet Astron. AJ (Engl. Transl.), 10, 602 (1967).

C. J. Hogan and M. J. Rees, "AXION MINICLUSTERS," Phys. Lett. B **205** (1988), 228-230

V. S. Berezinsky, V. I. Dokuchaev and Y. N. Eroshenko, "Formation and internal structure of superdense dark matter clumps and ultracompact minihaloes," JCAP **11** (2013), 059 [arXiv:1308.6742 [astro-ph.CO]].

K. Freese, T. Rindler-Daller, D. Spolyar and M. Valluri, "Dark Stars: A Review," Rept. Prog. Phys. **79** (2016) no.6, 066902 [arXiv:1501.02394 [astro-ph.CO]].

Li G., Adams F., "Cross-sections for planetary systems interacting with passing stars and binaries". 2015, MNRAS, 448, 344.

Spurzem R., Giersz M., Heggie D. C., Lin D. N. C., "Dynamics of Planetary Systems in Star Clusters" 2009, ApJ, 697, 458.

J. F. Navarro, C. S. Frenk and S. D. M. White, "A Universal density profile from hierarchical clustering," Astrophys. J. **490** (1997), 493-508 [arXiv:astro-ph/9611107 [astro-ph]].

Cuello N., Ménard F., Price D. J., "How stellar flybys shape planet-forming discs". 2022, arXiv, arXiv:2207.09752

Moore N. W. H., Li G., Adams F. C., "Inclination Excitation of Solar System Debris Disk Due to Stellar Flybys". 2020, ApJ, 901, 92.

Hills J. G., "Encounters between binary and single stars and their effect on the dynamical evolution of stellar systems." 1975, AJ, 80, 809.

Mayor, M. and Queloz, D., "A Jupiter-mass companion to a solar-type star", Nature, vol. 378, no. 6555, pp. 355-359, 1995.

The ExtrasolarPlanets Encyclopedia: `http://exoplanet.eu/`

Burke, C. J., "Terrestrial Planet Occurrence Rates for the Kepler GK Dwarf Sample", The Astrophysical Journal, vol. 809, no. 1, 2015.

Christiansen et al., "Measuring Transit Signal Recovery in the Kepler Pipeline. III. Completeness of the Q1-Q17 DR24 Planet Candidate Catalogue with Important Caveats for Occurrence Rate Calculations", The Astrophysical Journal, vol. 828, no. 2, 2016.

Mulders, G. D., O'Brien, D. P., Ciesla, F. J., Apai, D., and Pascucci, I., "Earths in Other Solar Systems' N-body Simulations: The Role of Orbital Damping in Reproducing the Kepler Planetary Systems", The Astrophysical Journal, vol. 897, no. 1, 2020.

Emsenhuber, A., Mordasini, C., Burn, R., Alibert, Y., Benz, W., and Asphaug, E., "The New Generation Planetary Population Synthesis (NGPPS). I. Bern global model of planet formation and evolution, model tests, and emerging planetary systems", Astronomy and Astrophysics, vol. 656, 2021.

Chandrasekhar, S., "Dynamical Friction. I. General Considerations: the Coefficient of Dynamical Friction", The Astrophysical Journal, vol. 97, p. 255, 1943.

Rein, H., and S-F. Liu. "REBOUND: an open-source multi-purpose N-body code for collisional dynamics." Astronomy & Astrophysics 537 (2012): A128.

Brown, G. AIRBALL. `https://github.com/zyrxvo/airball`

Rein H., Tamayo D., "WHFast: a fast and unbiased implementation of a symplectic Wisdom-Holman integrator for long-term gravitational simulations". 2015, MNRAS, 452, 376.

Rein, H. and Spiegel, D. S., "IAS15: a fast, adaptive, high-order integrator for gravitational dynamics, accurate to machine precision over a billion orbits", Mon. Not. Roy. Astron. Soc., vol. 446, no. 2, pp. 1424-1437, 2015.

Price-Whelan, A., "Gala: A Python package for galactic dynamics," J. Open Source Softw., **2** (2017,10),

B. V. Lehmann, A. Webber, O. G. Ross and S. Profumo, "Capture of primordial black holes in extrasolar systems," JCAP **08** (2022), 079 [arXiv:2205.09756].

B. V. Lehmann, O. G. Ross, A. Webber and S. Profumo, "Three-body capture, ejection, and the demographics of bound objects in binary systems," Mon. Not. Roy. Astron. Soc. **505** (2021) no.1, 1017-1028 [arXiv:2012.05875].

F. C. Adams, "The Birth Environment of the Solar System," Ann. Rev. Astron. Astrophys. **48** (2010), 47-85 [arXiv:1001.5444].

Brown G., Rein H., "On the long-term stability of the Solar system in the presence of weak perturbations from stellar flybys". 2022, MNRAS, 515, 5942.

J. Bovy and S. Tremaine, "On the local dark matter density," Astrophys. J. **756** (2012), 89 [arXiv:1205.4033].

B. Carr and F. Kuhnel, "Primordial Black Holes as Dark Matter: Recent Developments," Ann. Rev. Nucl. Part. Sci. **70** (2020), 355-394 [arXiv:2006.02838].

C. Chen and Y. F. Cai, "Primordial black holes from sound speed resonance in the inflaton-curvaton mixed scenario," JCAP **10** (2019), 068 [arXiv:1908.03942].

Magaña J., et al. "Extended primordial black hole mass functions with a spike". 2022, arXiv, arXiv:2207.13689

Rein H., Liu S.-F., "REBOUND: an open-source multi-purpose N-body code for collisional dynamics". 2012, A&A, 537, A128.

Yang B., Walker K. M., Forrey R. C., Stancil P. C., Balakrishnan N., "Collisional quenching of highly rotationally excited HF" 2015, A&A, 578, A65.